THE LANCET
Planetary Health

Supplementary appendix

This appendix formed part of the original submission and has been peer reviewed. We post it as supplied by the authors.

Supplement to: Wei J, Wang J, Li Z, et al. Long-term mortality burden trends attributed to black carbon and $PM_{2·5}$ from wildfire emissions across the continental USA from 2000 to 2020: a deep learning modelling study. *Lancet Planet Health* 2023; **7:** e963–75.

Supplemental Appendix

Long-term mortality burden trends attributed to black carbon and $PM_{2.5}$ from wildfire emissions across the continental US from 2000-2020: a deep learning modelling study

Jing Wei PhD [1,2*], Prof Jun Wang PhD [1*], Prof Zhanqing Li PhD [2*], Shobha Kondragunta PhD [3], Prof Susan Anenberg PhD [4], Prof Yi Wang PhD [1], Huanxin Zhang PhD [1], David Diner PhD [5], Jenny Hand PhD [6], Alexei Lyapustin PhD [7], Ralph Kahn PhD [7], Peter Colarco PhD [8], Arlindo da Silva PhD [9], Prof Charles Ichoku PhD [10]

1. Department of Chemical and Biochemical Engineering, Iowa Technology Institute, Center for Global and Regional Environmental Research, University of Iowa, Iowa City, IA 52242, USA
2. Department of Atmospheric and Oceanic Science, Earth System Science Interdisciplinary Center, University of Maryland, College Park, MD 20472, USA
3. Center for Satellite Applications and Research, NOAA National Environmental Satellite, Data, and Information Service, College Park, MD 20740, USA
4. Department of Environmental and Occupational Health, George Washington University, Washington, DC 20052, USA
5. Jet Propulsion Laboratory, California Institute of Technology, Pasadena, CA 91109, USA
6. Cooperative Institute for Research in the Atmosphere, Colorado State University, Fort Collins, CO 80523, USA
7. Climate and Radiation Laboratory, NASA Goddard Space Flight Center, Greenbelt, MD 20771, USA
8. Atmospheric Chemistry and Dynamics Laboratory, NASA Goddard Space Flight Center, Greenbelt, MD 20771, USA
9. Global Modeling and Assimilation Office, NASA Goddard Space Flight Center, Greenbelt, MD 20771, USA
10. Department of Geography and Environmental Systems, University of Maryland Baltimore County, Baltimore, MD 21250, USA

*Corresponding authors:

Jun Wang, jun-wang-1@uiowa.edu; Zhanqing Li, zhanqing@umd.edu;

Jing Wei: weijing@umd.edu

Table of Contents

Appendix Texts

Text S1: Spatiotemporally Weighted Deep Forest model

Air pollution usually shows significant spatiotemporal variations. Autocorrelations of $PM_{2.5}$ or BC data are often strong and positive in locations or at times that are close to each other. Such autocorrelations are weakened or disappear as the spatial or temporal distances increase. The autocorrelations are also not uniform with space and time, suggesting that the relative weights in combining different datasets to predict surface $PM_{2.5}$ or BC should vary dynamically with time and space. Therefore, the spatiotemporally weighted deep forest (SWDF) model was developed to improve both the accuracy and the spatial continuity of the prediction of $PM_{2.5}$ and BC.[1] Here, we conducted separate training of the SWDF models for $PM_{2.5}$ and BC by utilizing data samples collected during the study period (2000–2020).

As shown in the flowchart (Figure S2), $PM_{2.5}$ and BC estimates were conducted by training the SWDF model in multiple stages with surface $PM_{2.5}$ and BC measurements as targets and their spatiotemporally paired big data as features, including satellite remote sensing products, model simulations, meteorology reanalysis, and anthropogenic emissions.

Stage I: The input features for the SWDF model to predict $PM_{2.5}$ were collected, including daily MAIAC and MERRA2 AODs and other auxiliary variables, including MERRA2-$PM_{2.5}$ components (i.e., surface mass concentrations of BC, organic carbon, dust, sulfate, and sea salt); nine ERA5 meteorological fields (i.e., temperature, precipitation, u- and v-components of wind, surface pressure, boundary layer height, and relative humidity); anthropogenic emissions of $PM_{2.5}$ precursors (i.e., nitrogen oxide, ammonia, sulfur dioxide, and volatile organic compounds); normalized difference vegetation index; digital elevation model; and population density (Equation 1).

Stage II: BC concentrations were then separately derived from the $PM_{2.5}$ estimates by further combining surface observations, satellite data, and model outputs on a daily basis for each year using the SWDF model. In addition to the same meteorological and surface variables used for predicting $PM_{2.5}$, also adopted for the prediction of BC were MISR and MERRA2 absorbing

AODs, MERRA2 BC AOD, BC surface mass concentrations, and natural and anthropogenic BC emissions (Equation 2).

Mathematically, stages I and II are described as:

$$PM_{2.5(ijt)} \sim f_{\mathrm{SWDF}}(SAOD_{ijt}, MAOD_{ijt}, Component_{ijt}, PMEM_{ijm}, Meteorology_{ijt}, NDVI_{ijm}, DEM_{ijy}, POP_{ijy}, P_s, P_t), \quad (1)$$

$$BC_{ijt} \sim f_{\mathrm{SWDF}}(FPM_{2.5(ijt)}, BCSM_{ijt}, BCAOD_{ijt}, MAAOD_{ijm}, SAAOD_{ijm}, BCEM_{ijm}, Meteorology_{ijt}, NDVI_{ijm}, DEM_{ijy}, POP_{ijy}, P_s, P_t), \quad (2)$$

where $PM_{2.5(ijt)}$ and BC_{ijt} indicate the ground-based $PM_{2.5}$ and BC measurements for one grid box (i, j) on the t^{th} day of a year; $SAOD_{ijt}$ and $MAOD_{ijt}$ indicate the MAIAC and MERRA2 AODs, respectively; $FPM_{2.5(ijt)}$ represents the full-coverage $PM_{2.5}$ predictions; $Component_{ijt}$ and $Meteorology_{ijt}$ represent the MERRA2 $PM_{2.5}$ components and ERA5 meteorological fields, respectively; $PMEM_{ijm}$ and $BCEM_{ijm}$ represent the emissions contributing to $PM_{2.5}$ and BC, respectively; $BCSM_{ijt}$, $BCAOD_{ijt}$, and $MAAOD_{ijm}$ and represent the MERRA2 BC surface mass concentration, BC AOD, and absorbing AOD, respectively; $SAAOD_{ijm}$ and $NDVI_{ijm}$ represent the MISR absorbing AOD and normalized difference vegetation index, respectively; DEM_{ij} and POP_{ijy} represent the annual digital elevation model and population density, respectively; P_s and P_t represent the spatial and temporal terms, where P_s is characterized by:

$$P_s \sim (Lon, Lat, W_{s(ul)}, W_{s(um)}, W_{s(ur)}, W_{s(rm)}, W_{s(br)}, W_{s(bm)}, W_{s(bl)}, W_{s(lm)}, W_{s(ct)}), \quad (3)$$

$$W_{s(mn)} = \frac{1}{\sqrt{D_{\mathrm{Haversine}(mn)}}}, \quad (4)$$

where Lon and Lat represent the longitude and latitude of one grid box in the continental US; $W_{s(ul)}, W_{s(um)}, W_{s(ur)}, W_{s(rm)}, W_{s(br)}, W_{s(bm)}, W_{s(bl)}, W_{s(lm)}$ and $W_{s(ct)}$ represent the spatial weight factors, i.e., the inverse of the square root of Haversine great-circle distances (unit: km) from the center of one point in space to the center of the grid boxes in the upper-left, upper-

middle, upper-right, right-middle, bottom-right, bottom-middle, bottom-left, and left-middle directions and the center of the continental US, respectively. Similarly, P_t is characterized by:

$$P_t \sim (DOY, W_{t(se)}, W_{t(ss)}, W_{t(ae)}, W_{t(ws)}), \quad (5)$$

$$W_{t(mn)} = \frac{1}{D_{mn}}, \quad (6)$$

where DOY represents the day of the year; $W_{t(se)}, W_{t(ss)}, W_{t(ae)}$, and $W_{t(ws)}$ represent the temporal weight factors, and D_{mn} is the inverse distances (unit: day) from that day to the spring equinox, summer solstice, autumn equinox, and winter solstice, respectively.

Text S2: Calculation of the mortality burden

The long-term mortality impact of ambient air pollution is assessed at each 1-km^2 grid in the continental US by utilizing annual mean concentrations of $PM_{2.5}$ and BC from 2000 to 2020. The concentration-response functions for the mortality analysis are expressed as the log-linear relationship between relative risk (RR) and related changes in concentrations of air pollutants ($PM_{2.5}$ and BC):[2-4]

$$RR(x) = \begin{cases} 1, & x < x_0 \\ e^{\beta \Delta x}, & x \geq x_0 \end{cases} \quad , \qquad (7)$$

where β is the concentration–response coefficient (estimated as the increase in all-cause mortality per unit increase in pollutant concentration), and Δx represents the difference between the current pollutant concentration (x) and the target or threshold pollutant concentration (x_0). We select x_0 according to the Theoretical Minimum Risk Exposure Level (TMREL). Following the recent GBD 2019 study,[5] the TMREL for $PM_{2.5}$ ranges from 2.4 to 5.9 μg m^{-3}. Unlike $PM_{2.5}$, BC currently lacks a universal reference standard. As a result, we defined the TMREL for BC based on the minimum value to the fifth percentiles of annual BC distributions, following a similar determination method used in the GBD study[5] and previous studies.[6,7]

The all-cause mortality burden (MB) associated with long-term exposure to $PM_{2.5}$ and BC in a given year can be subsequently estimated by using the RR, baseline mortality rate (BMR), and population density (POP):

$$MB = \frac{RR-1}{RR} \times BMR \times POP \qquad (8)$$

The baseline mortality and population are collected from the United Nations - World Population Prospects and LandScan™ global population databases at a 1-km resolution, respectively.[8]

In sensitivity experiments considering the larger toxicity of BC, the mortality burden assessment is a three-step process. First, the BC mass is subtracted from the total $PM_{2.5}$ to avoid double counting. Subsequently, the mortality burden associated with non-BC $PM_{2.5}$ mass, or

$MB_{PM_{2.5}-BC}$, is calculated using the $PM_{2.5}$ RR from the Pope et al. (2019) study.[9] Second, the mortality burden specifically attributed to BC (MB_{BC}) is calculated separately using the pooled estimate of BC RR,[10] which captures the unique contribution of BC and its pronounced impact on health outcomes. Finally, the total mortality burden that considers the larger toxicity of BC (MB_{LT}) is obtained by summing these two parts (Equation 9). This approach ensures that the distinct role of BC is appropriately considered, resulting in a more thorough assessment of the health risks associated with BC-associated $PM_{2.5}$ exposure.

$$MB_{LT} = MB(RR_{PM_{2.5}})_{PM_{2.5}-BC} + MB(RR_{\mathrm{BC}})_{BC} \quad (9)$$

Text S3: Detection of the breakpoint

In this study, we utilize a well-established method for change point detection, which combines a time series analysis with a sliding window approach.[11,12] This allows us to identify a potential year within a specific period when an abnormal or reversed trend occurred:

$$S = \frac{min[p(P_l),p(P_r)]}{abs(P_l - P_r) * e(P_{l+r})} \quad , \qquad (10)$$

Where S is a change point score, p represents the probability of short-term trends for the left period (P_l) and right period (P_r) being insignificant, and e is the fitting error of the trend for the combined subseries (P_{l+r}). The probabilities and the statistical significance levels of the trends, which are determined using the least-squares linear regression method, are assessed using p-values based on the t-statistic in a two-sided hypothesis test. The year t is identified as a breakpoint when S reaches its lowest value or when a trend reversal with at least one-side significance surpasses the 90% confidence level ($p < 0.1$). To enhance the robustness of our analysis, we adopted a time window of 3 years to ensure that each side of the trend spans a minimum of 4 years, i.e., [t-3, t, t+3]; consequently, this approach enables us to effectively search for trend reversals within the period 2000–2020.

Text S4: Removal of wildfire-related $PM_{2.5}$

A two-step model is developed here by combining the Pauta criterion and the InterQuartile Range (IQR) method to remove outliers of wildfire-related $PM_{2.5}$ data from daily data:

Step I: We employ the Pauta criterion to identify the specific day when a severe wildfire event may occur in the western US, utilizing daily $PM_{2.5}$ wildfire emission data sourced from the Fire Energetics and Emissions Research (FEER) database. To mitigate the impact of extreme $PM_{2.5}$ concentrations associated with wildfires, we utilize medians instead of means plus one standard deviation as the threshold for filtering, based on statistics from all corresponding days of the year for all years spanning the entire study period from 2000 to 2020.

Step II: We adopt the IQR method to identify regions in the western US that are affected by heavy wildfires, employing our 1-km daily $PM_{2.5}$ predictions. The IQR method quantifies variability by dividing the data samples into quartiles, specifically by calculating the difference (Q3 – Q1) between the third quartile (Q3) and the first quartile (Q1). We set the threshold filter as 1.5 times the IQR to detect wildfire-related $PM_{2.5}$. Any data points that exceed this threshold are subsequently excluded from the calculation of the $PM_{2.5}$ time series.

While this approach is useful for identifying days with extreme wildfire smoke $PM_{2.5}$, it may miss days with a small additional amount in $PM_{2.5}$ originating from smoke. Future studies are needed to deploy process-oriented methods like chemistry transport modeling to quantify the contribution to $PM_{2.5}$ from fire emissions.

Text S5: Data Availability

The Environmental Protection Agency (EPA) and Interagency Monitoring of Protected Visual Environments (IMPROVE) $PM_{2.5}$ and BC measurements are available at https://www.epa.gov/aqs and http://views.cira.colostate.edu/fed/. The US Forest Service AirSis (USFS) and Western Regional Climate Center (WRCC) $PM_{2.5}$ measurements are available at https://haze.airfire.org/monitoring/. MODIS, MISR, and MERRA2 products are available at https://earthdata.nasa.gov/. CAMS global emission inventories are available at https://ads.atmosphere.copernicus.eu/. Fire Energetics and Emissions Research (FEER) is available at https://feer.gsfc.nasa.gov/. ERA5 global reanalysis is available at https://cds.climate.copernicus.eu/. The Shuttle Radar Topography Mission (SRTM) digital elevation model (DEM) is available at https://www2.jpl.nasa.gov/srtm/. LandScan^{TM} global population data is available at https://landscan.ornl.gov/.

Appendix Figures

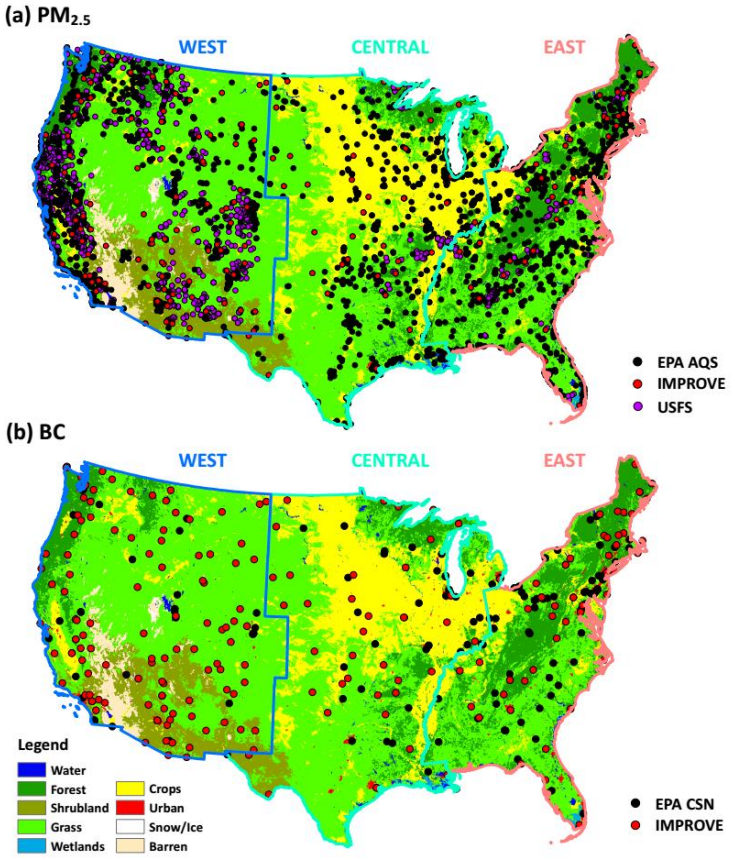

Figure S1. Geographical locations of ground-based stations that measure (a) $PM_{2.5}$ and (b) BC. These stations are color-coded based on their associated networks, including the Environmental Protection Agency (EPA) Air Quality System (AQS), the Chemical Speciation Monitoring Network (CSN), the Interagency Monitoring of Protected Visual Environments (IMPROVE), and the United States Forest Service (USFS) across the continental United States. The background-colored map indicates the land-use type. The colored boundaries define the areas of West, Central, and East United States, as referred to in the main text.

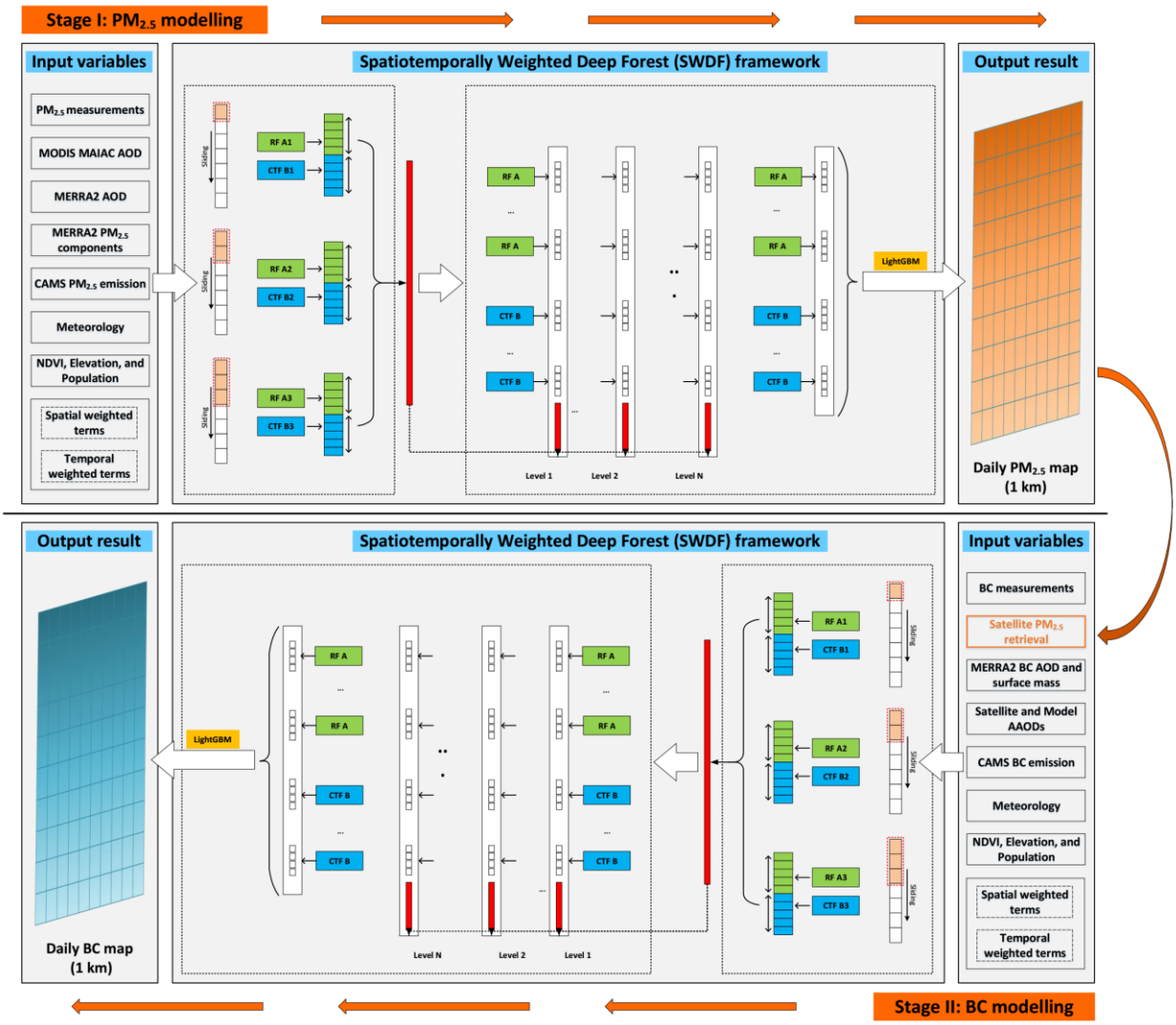

Figure S2. Flowchart of the developed spatiotemporally weighted deep forest (SWDF) model for estimating surface $PM_{2.5}$ and BC concentrations in this study.

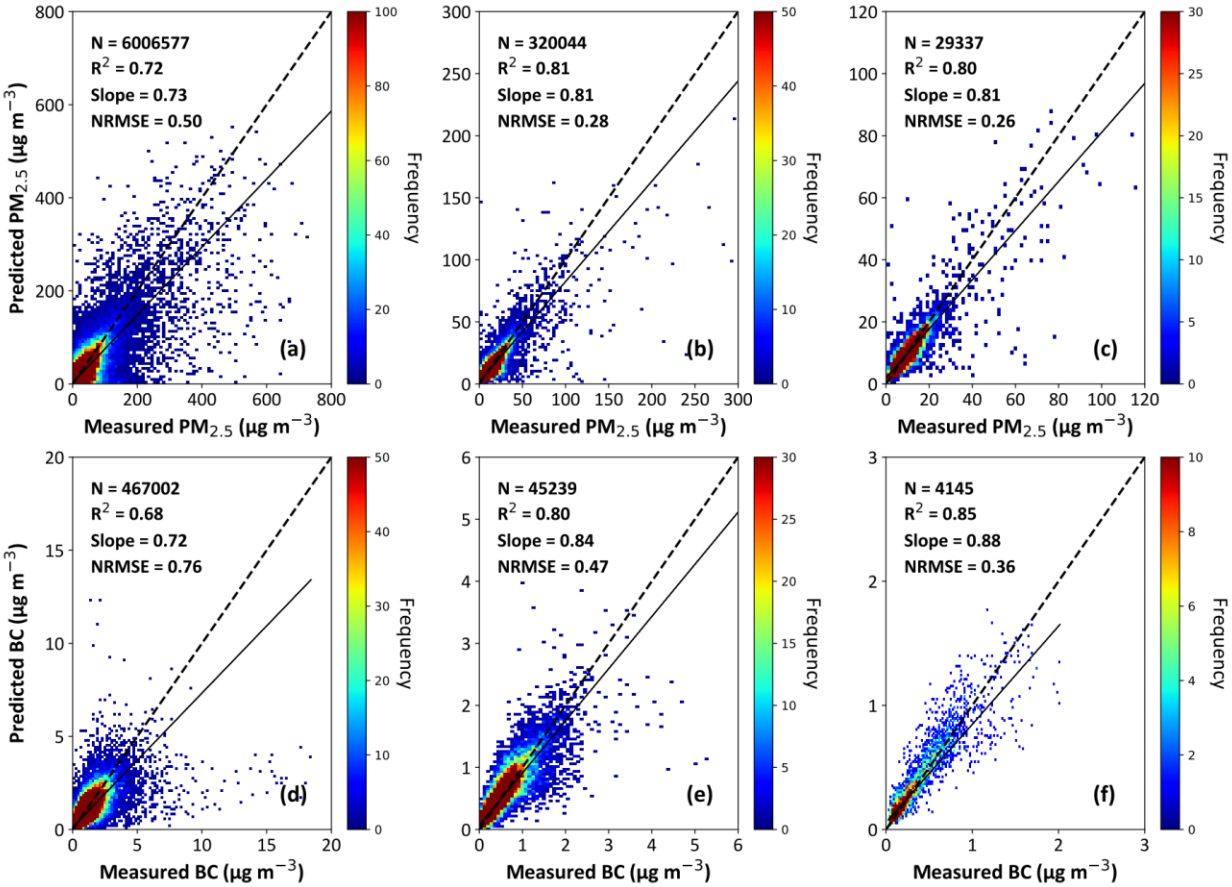

Figure S3. Spatial-based cross-validation of measured (x-axis) and predicted (y-axis) (a & d) daily, (b & e) monthly, and (c & f) annual $PM_{2.5}$ (top row) and BC (bottom row) concentrations (unit: μg m^{-3}) collected at all ground monitoring stations across the continental United States during the period 2000–2020. The colors in the scatter plot represent the density of data points that fall within a given grid (frequency). The black dashed lines are 1:1 lines, and black solid lines are best-fit lines from linear regression between the retrievals and measurements.

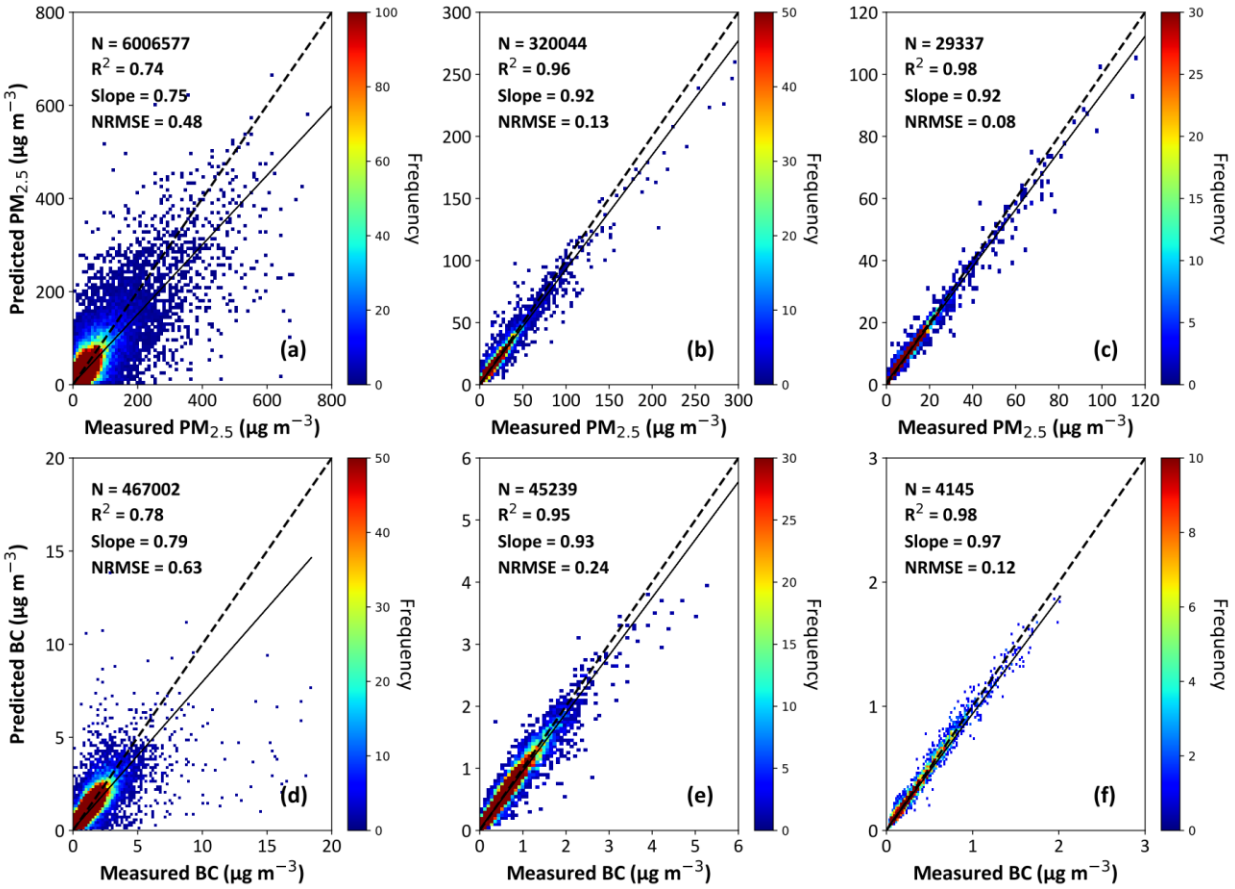

Figure S4. Temporal-based cross-validation of measured (x-axis) and predicted (y-axis) (a & d) daily, (b & e) monthly, and (c & f) annual $PM_{2.5}$ (top row) and BC (bottom row) concentrations (unit: μg m^{-3}) collected at all ground monitoring stations across the continental United States during the period 2000–2020. The colors in the scatter plot represent the density of data points that fall within a given grid (frequency). The black dashed lines are 1:1 lines, and black solid lines are best-fit lines from linear regression between the retrievals and measurements.

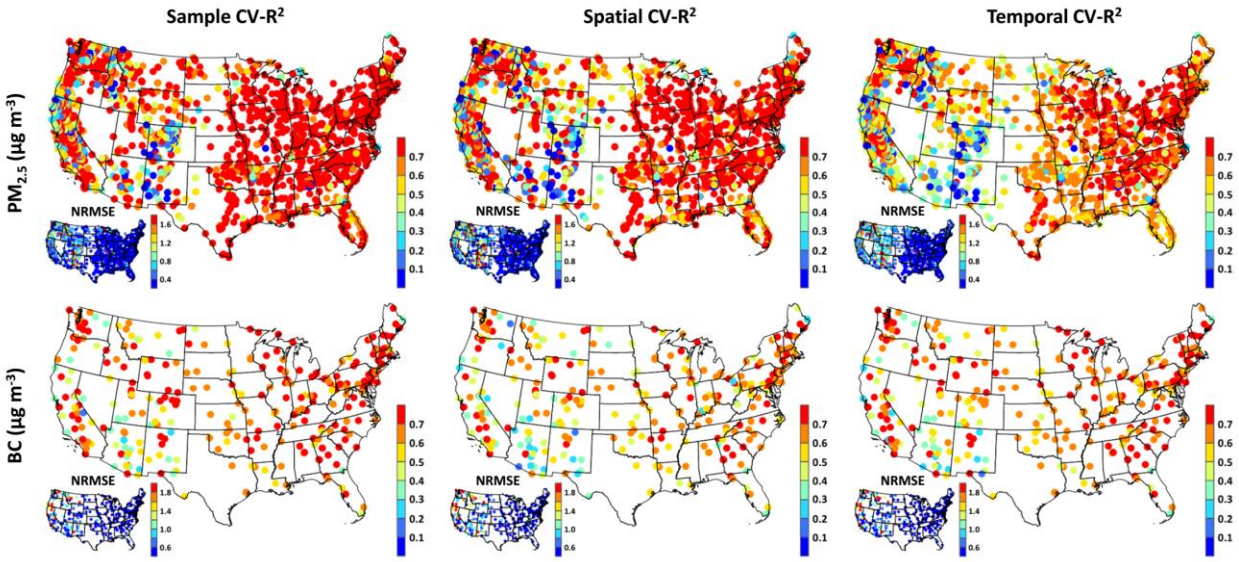

Figure S5. Spatial distribution of model performance at different surface stations. The performance is assessed by sample-based (left panels), spatial-based (central panels), and temporal-based (right panels) cross-validation of daily $PM_{2.5}$ (top row) and BC (bottom row) retrievals (unit: μg m^{-3}) against ground measurements (unit: μg m^{-3}) for each monitoring station across the continental United States during the period 2000–2020. Note that only stations with at least 30 samples are shown for statistical significance. Small maps in the lower left of each panel show normalized root mean square errors (NRMSE).

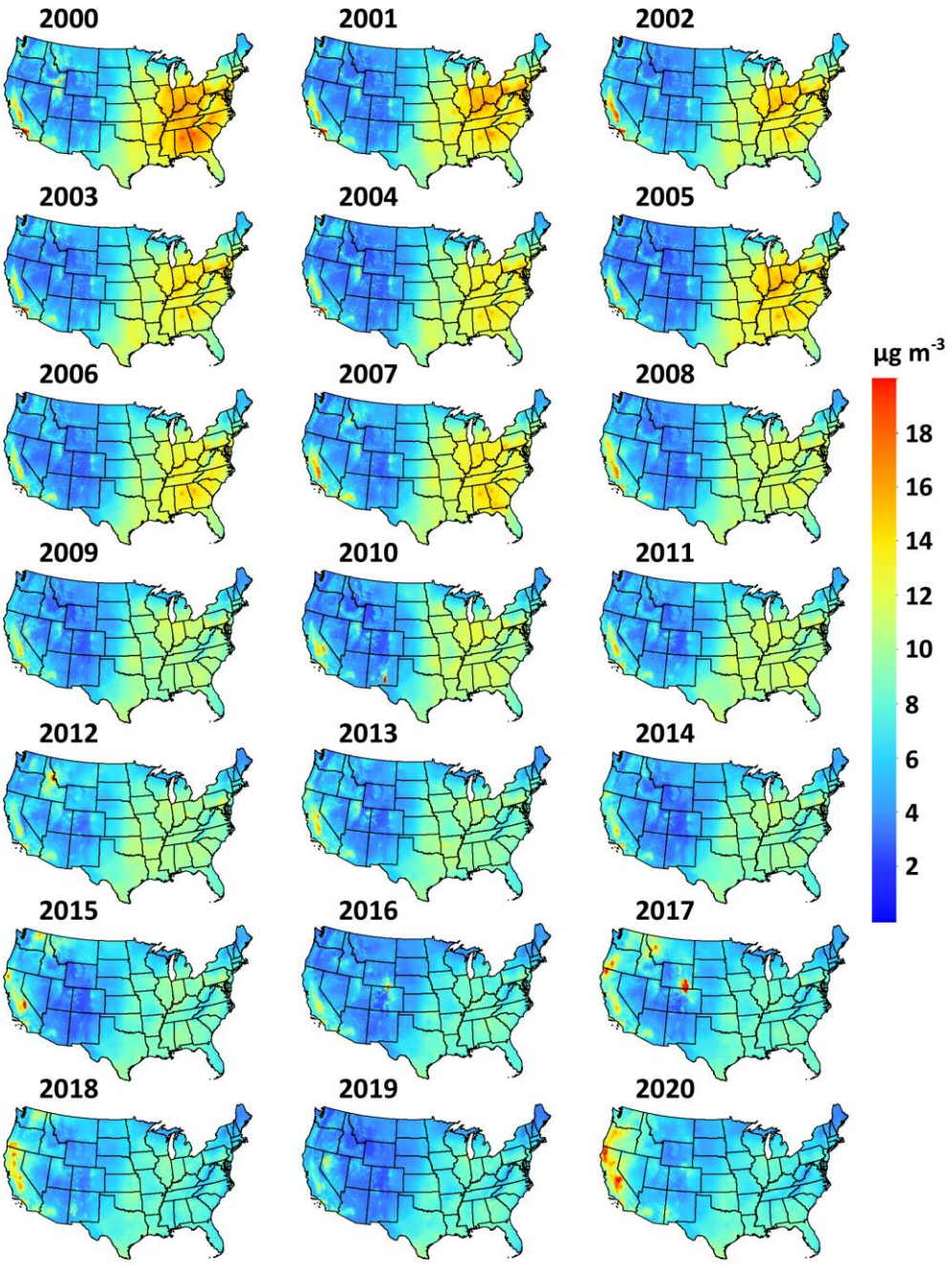

Figure S6. Spatial distributions of annual mean $PM_{2.5}$ concentrations (unit: μg m^{-3}) for each year from 2000 to 2020 at each 1-km^2 grid across the continental US.

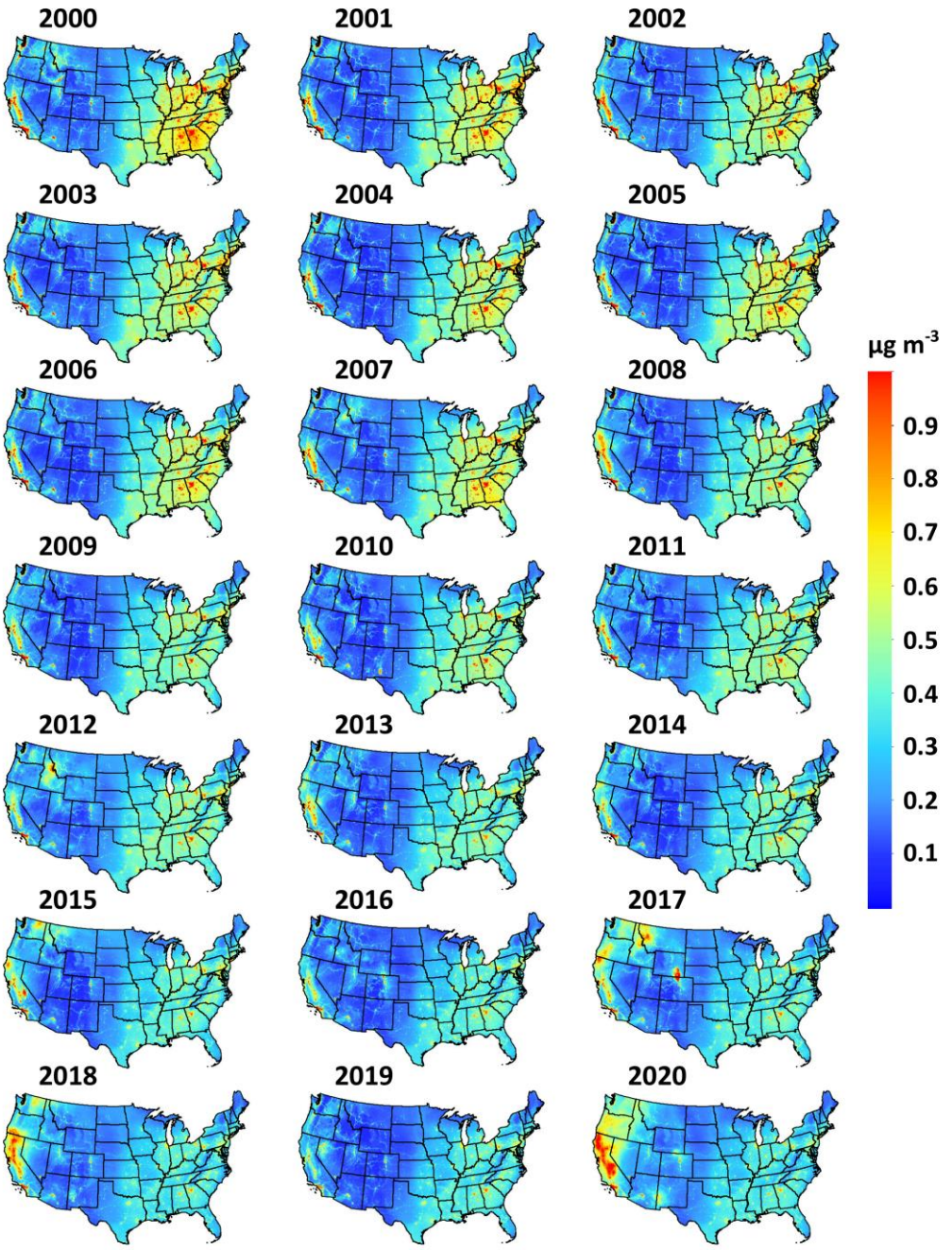

Figure S7. Spatial distributions of annual mean BC concentrations (unit: μg m^{-3}) for each year from 2000 to 2020 at each 1-km^2 grid across the continental US.

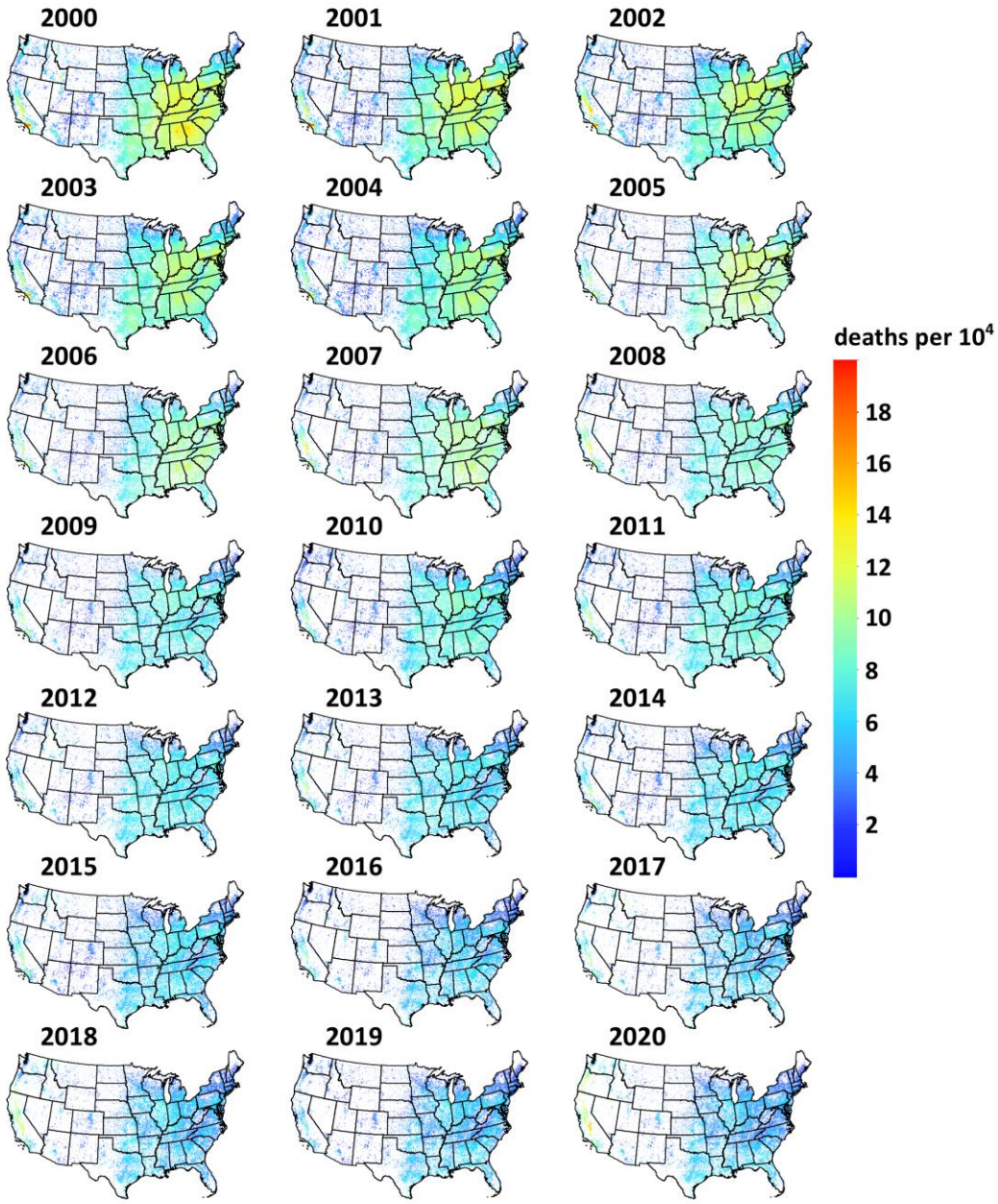

Figure S8. Spatial distributions of $PM_{2.5}$-associated death rate (unit: deaths per 10,000 people) for each year from 2000 to 2020 at each 1-km^2 grid across the continental US.

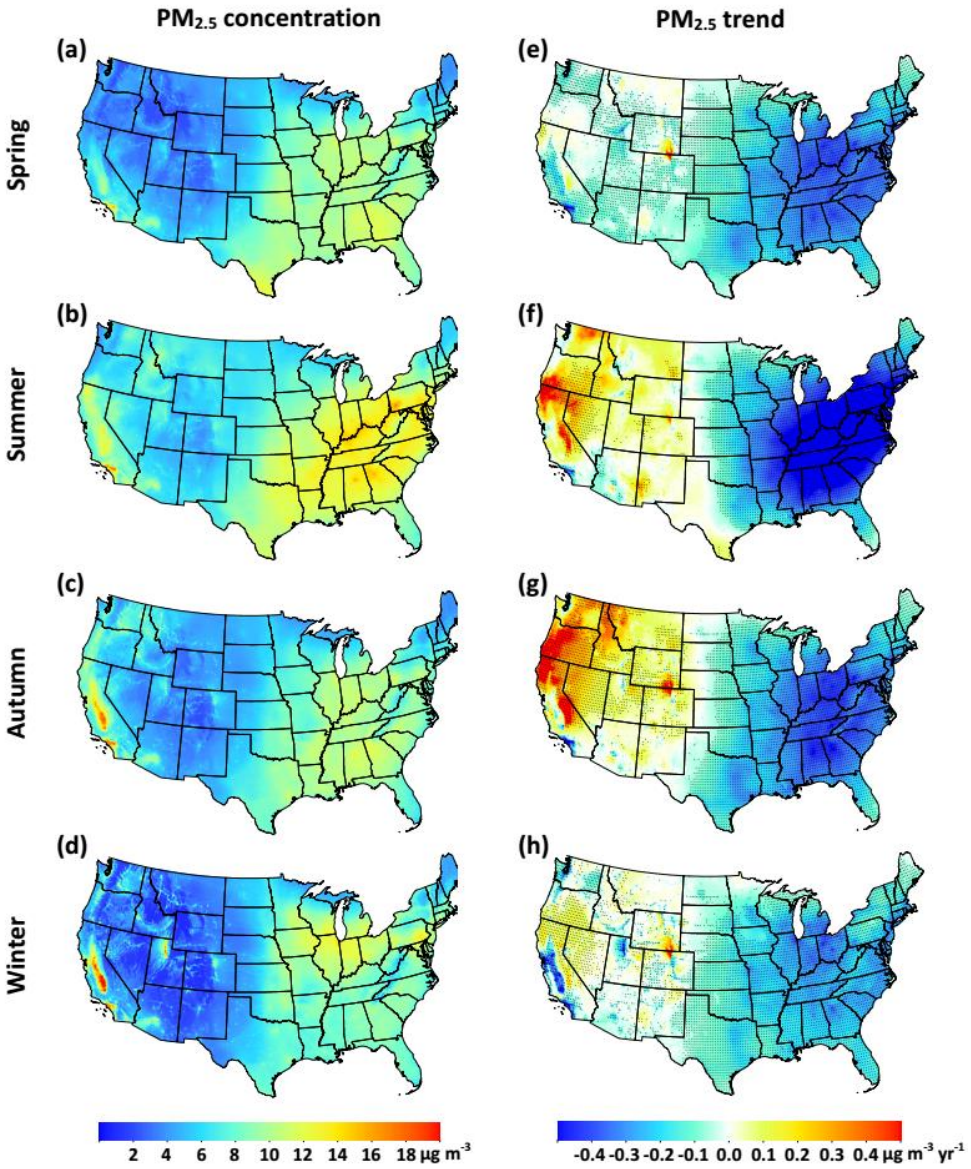

Figure S9. Spatial distributions of (a-d) seasonal mean (unit: μg m^{-3}) and (e-h) temporal trends (unit: μg m^{-3} yr^{-1}) of $PM_{2.5}$ concentrations from 2000 to 2020 across the continental United States. Each black dot in (e-h) represents a 30-km^2 area where the trend is significant at the 95% ($p < 0.05$) confidence level.

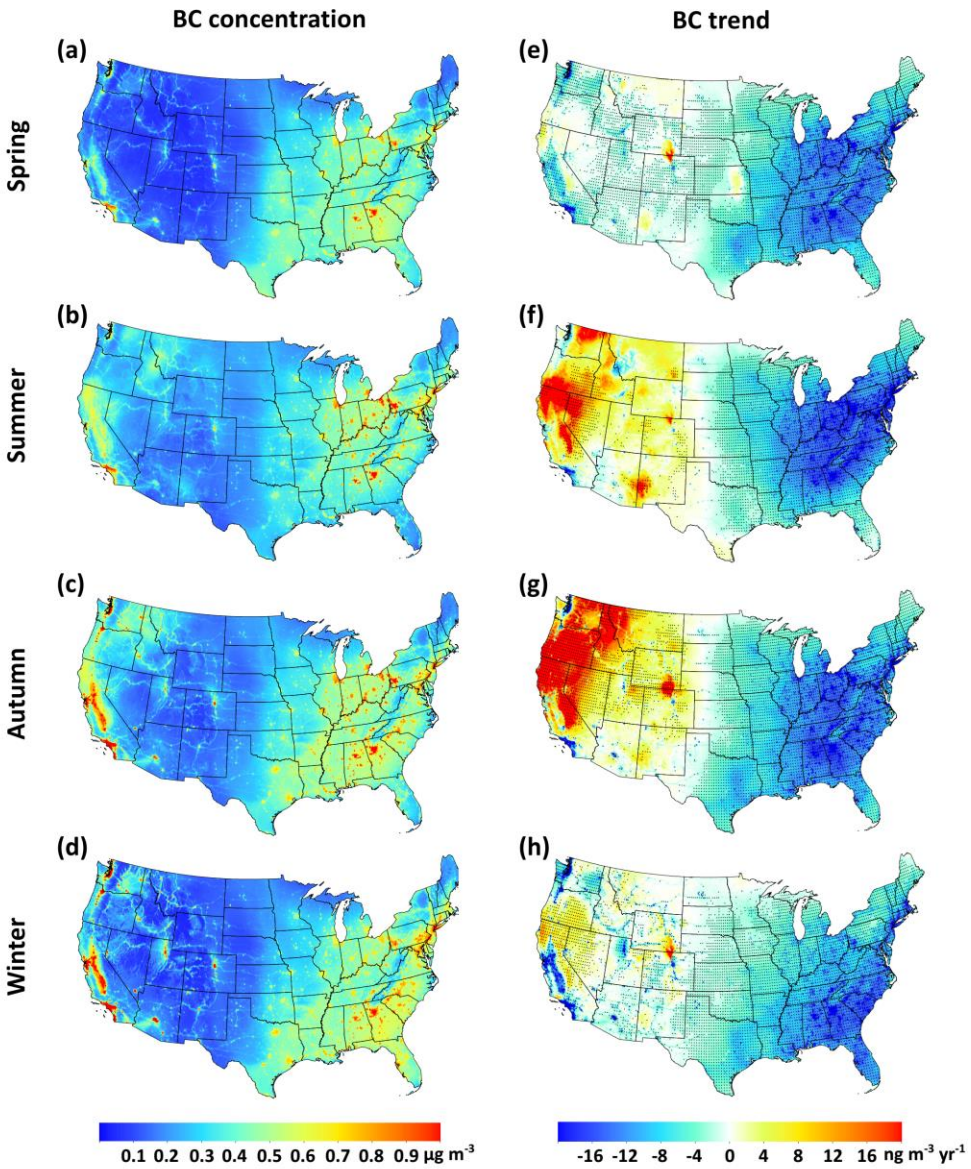

Figure S10. Spatial distributions of (a-d) seasonal mean (unit: μg m^{-3}) and (e-h) temporal trends (unit: ng m^{-3} yr^{-1}) of BC concentrations from 2000 to 2020 across the continental United States. Each black dot in (e-h) represents a 30-km^2 area where the trend is significant at the 95% ($p < 0.05$) confidence level.

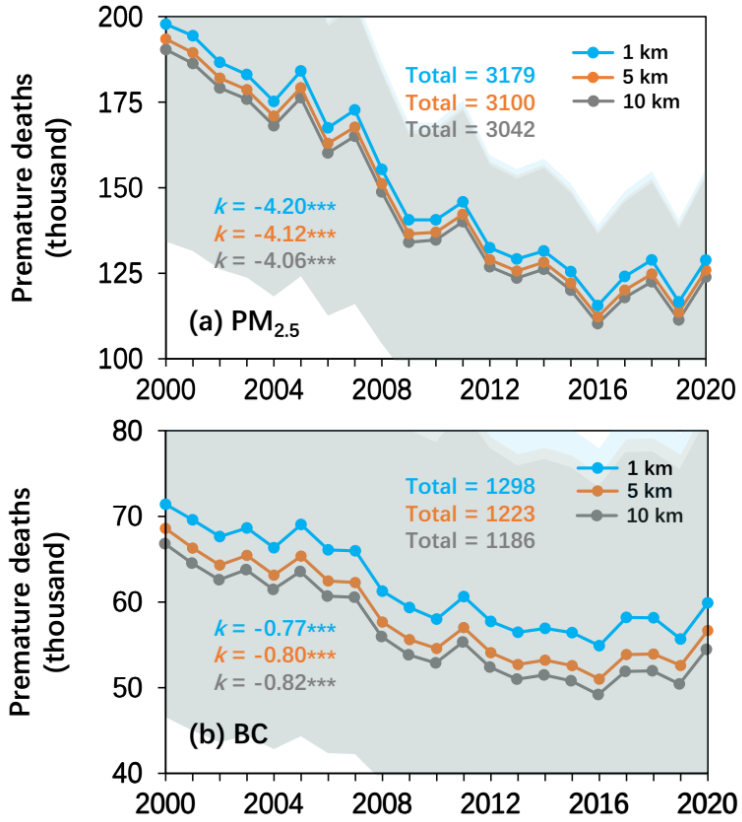

Figure S11. Sensitivity analysis of the impact of satellite retrievals of (a) $PM_{2.5}$ and (b) BC at various spatial resolutions (1, 5, and 10 km, indicated by colored solid lines) on the assessment of mortality burden in the continental US. The shaded areas represent confidence intervals ($p < 0.05$) on the estimated premature deaths. Total premature deaths (Total, unit: thousand) are given, and regressed slope (k) values are also provided, with *** representing trends that are significant at the 99% ($p < 0.01$) confidence level.

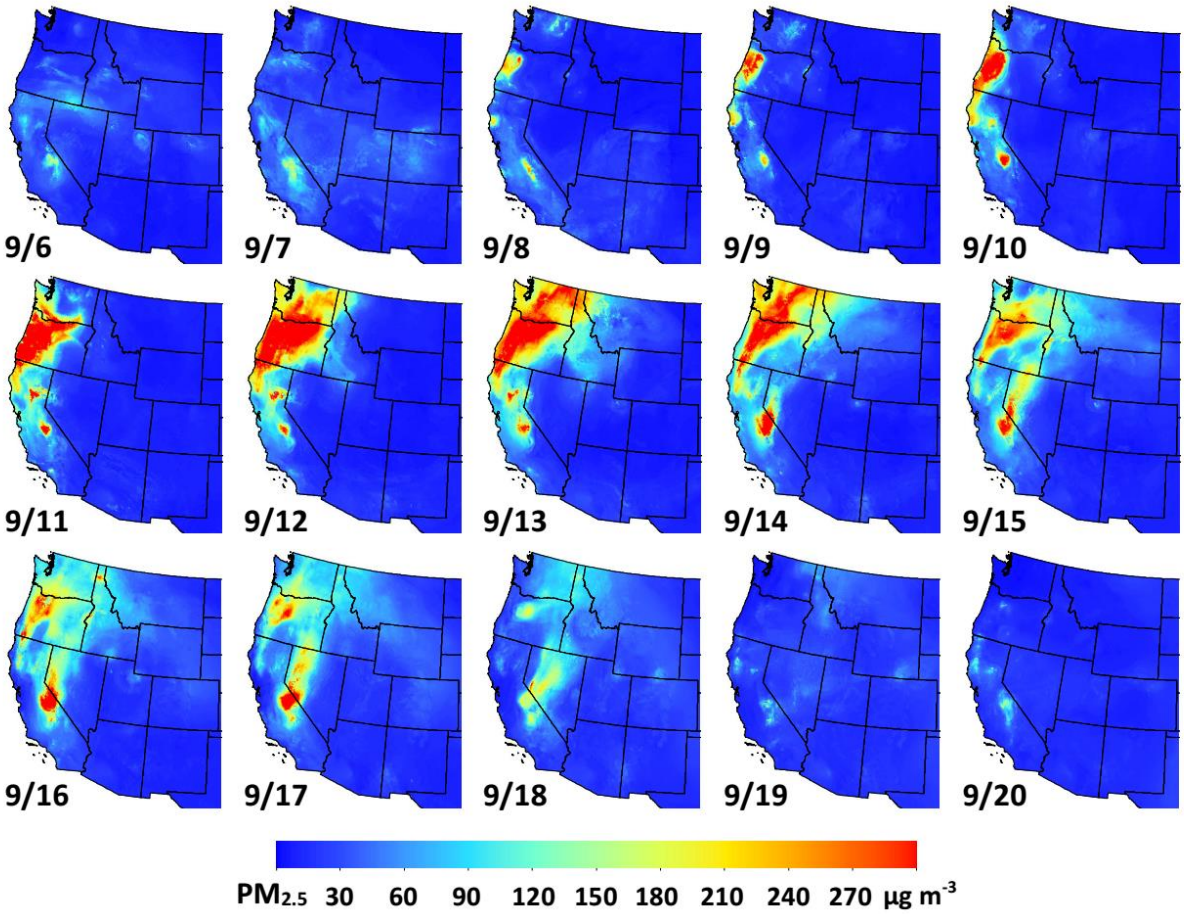

Figure S12. Spatial distributions of daily $PM_{2.5}$ maps (1-km resolution) during a severe wildfire event that occurred from 9 September to 20 September 2020 in the western United States.

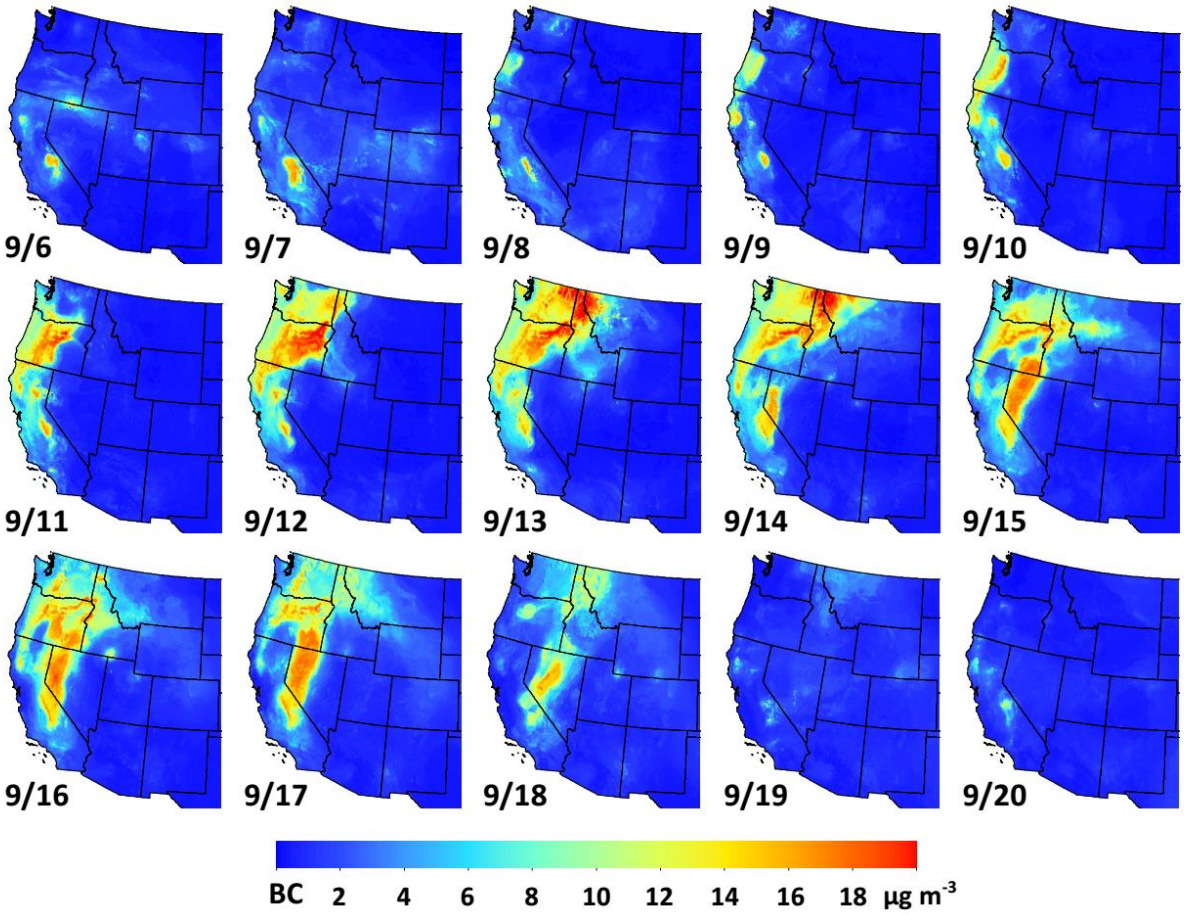

Figure S13. Spatial distributions of daily BC maps (1-km resolution) during a severe wildfire event that occurred from 9 September to 20 September 2020 in the western United States.

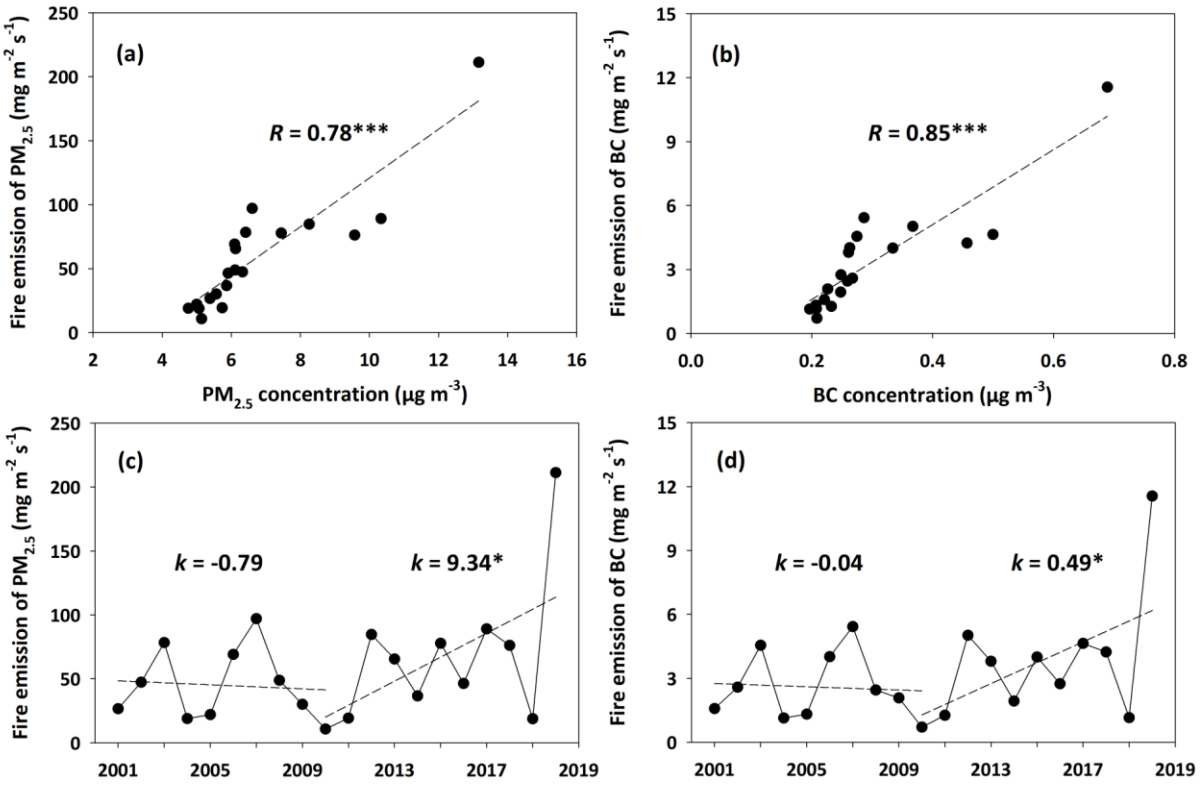

Figure S14. Correlations between (a) $PM_{2.5}$ and (b) BC concentrations (unit: μg m^{-3}) and their respective annual emissions (units: mg m^{-2} s^{-1}) from fires based on the Fire Energetics and Emissions Research (FEER) database[13], and time series of fire emissions of (c) $PM_{2.5}$ and (d) BC during the fire season (July–October) from 2001 to 2020 in the western US. Dashed lines represent regression lines, and the correlation coefficient (*R*) and slope (*k*) are given, where *, **, and *** represent correlations and trends that are significant at the 90% ($p < 0.1$), 95% ($p < 0.05$), and 99% ($p < 0.01$) confidence levels, respectively.

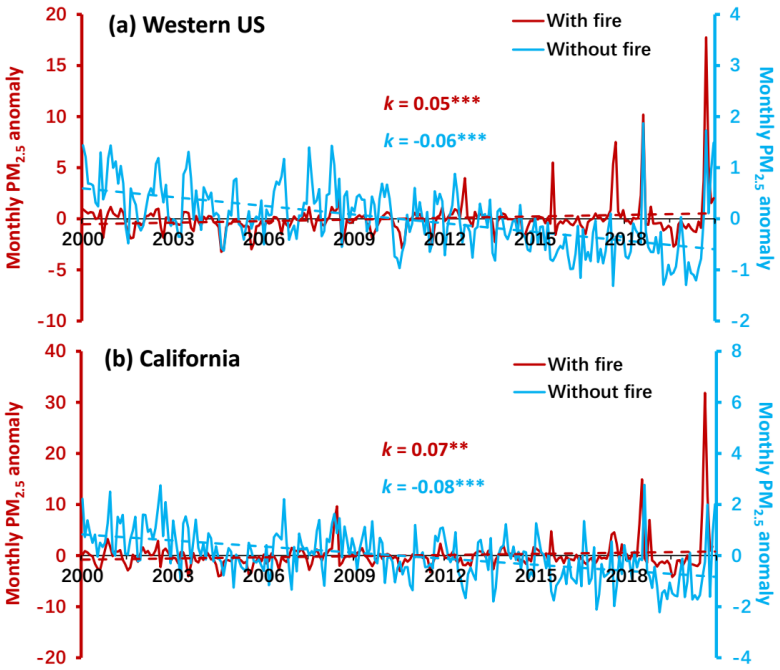

Figure S15. Time series of monthly $PM_{2.5}$ anomalies (defined as the difference between the monthly mean within a specific year and the monthly average value over the entire period of 2000–2020)[14] before (crimson lines) and after (blue lines) removing the daily outliers influenced by intense wildfire events from the monthly averages for each year from 2000 to 2020 in the (a) western US and (b) California. Regression lines are colored by region, and their slope (k, units: μg m^{-3} yr^{-1}) values are given, with *, **, and ***, representing trends that are significant at the 90% ($p < 0.1$), 95% ($p < 0.05$), and 99% ($p < 0.01$) confidence levels, respectively.

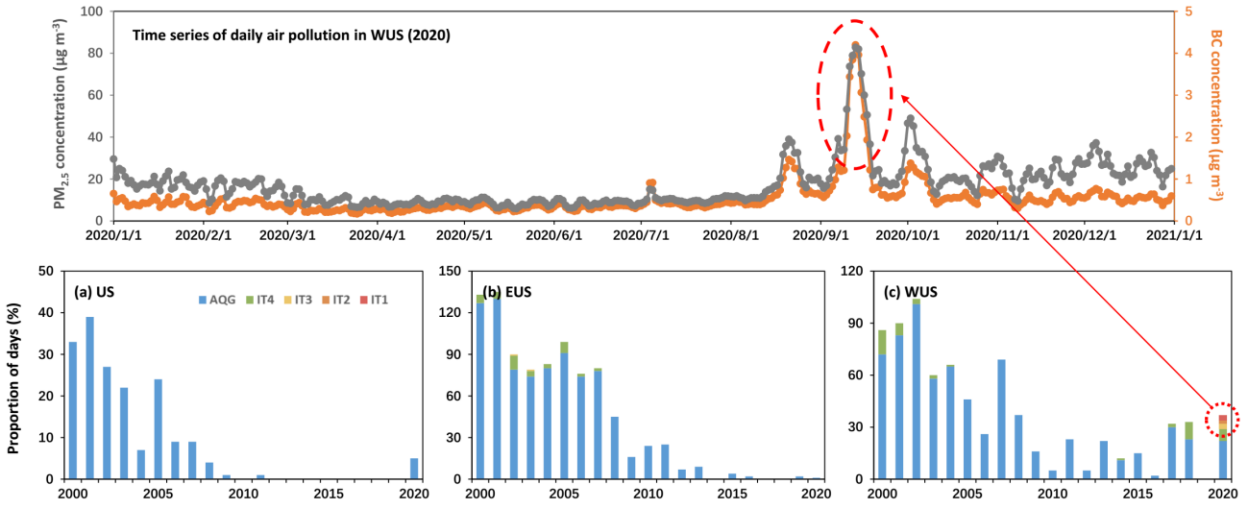

Figure S16. Time series of percentages of the days (unit: %) exceeding the World Health Organization (WHO) recommended short-term four interim targets (IT1: daily $PM_{2.5}$ = 75 μg m^{-3}), IT2: daily $PM_{2.5}$ = 50 μg m^{-3}, IT3: daily $PM_{2.5}$ = 37.5 μg m^{-3}, and IT4: daily $PM_{2.5}$ = 25 μg m^{-3}) and air quality guideline (AQG) level (daily $PM_{2.5}$ = 15 μg m^{-3}) in each year from 2000 to 2020 in the (a) continental United States (US), (b) eastern US (EUS), and (c) western US (WUS). The top panel shows time series of daily population-weighted mean $PM_{2.5}$ and BC concentrations (unit: μg m^{-3}) in 2020 in the WUS, where the red dashed ellipse outlines days with anomalously heavy pollution.

Appendix Tables

Table S1. Summary of data sources used in this study.

Category	Scientific Dataset	Spatial Resolution	Temporal Resolution	Data Source	Literature
Ground measurements	$PM_{2.5}$	In situ	Daily	EPA, IMPROVE, USFS	[15-17]
	BC	In situ	Hourly	CSN, IMPROVE	[16]
Satellite remote sensing product	MAIAC AOD	1 km	Daily	MCD19A2	[18]
	Absorbing AOD	0.5 °×0.5 °	Monthly	MISR	[19]
	NDVI	1 km	Monthly	MOD13A3	[20]
	Elevation	90 m	-	SRTM	[21]
	Population distribution	1 km	Annual	LandScan™	[8]
Chemical model simulation	Total aerosol extinction AOD Absorbing AOD Black carbon extinction AOD BC surface mass concentration OC surface mass concentration SO_4 surface mass concentration Dust surface mass concentration Sea salt surface mass concentration	0.625 °×0.5 °	1-hour	MERRA2	[22,23]
Emission inventory	Black carbon Ammonia Nitrogen oxides Sulphur dioxide Volatile organic compounds	0.1 °×0.1 °	Monthly	CAMS	[24]
	Smoke emissions	0.5 °×0.5 ° and 0.1 °×0.1 °	Monthly	FEER	[13]
Meteorological data	2-m air temperature Total precipitation 10-m u-component 10-m v-component Surface pressure	0.1 °×0.1 °	Hourly	ERA5-Land	[25]
	Boundary layer height Relative humidity	0.25 °×0.25 °	Hourly	ERA5	[26]

Table S2. Statistics of sample-based, spatial-based, and temporal-based cross-validated (CV) results between satellite-derived and ground-measured $PM_{2.5}$ and BC concentrations ($\mu g\ m^{-3}$) in the continental United States (US), East US (EUS), Central US (CUS), and West US (WUS) at daily, monthly, and yearly levels.

$PM_{2.5}$	Sample CV [R^2 (NRMSE)]			Spatial CV [R^2 (NRMSE)]			Temporal CV [R^2 (NRMSE)]		
	Daily	Monthly	Yearly	Daily	Monthly	Yearly	Daily	Monthly	Yearly
US	0.82 (0.40)	0.97 (0.11)	0.99 (0.07)	0.72 (0.49)	0.81 (0.28)	0.80 (0.26)	0.73 (0.48)	0.96 (0.13)	0.98 (0.08)
EUS	0.85 (0.24)	0.97 (0.07)	0.99 (0.03)	0.81 (0.28)	0.89 (0.14)	0.90 (0.10)	0.75 (0.32)	0.96 (0.09)	0.99 (0.04)
CUS	0.84 (0.26)	0.97 (0.07)	0.99 (0.03)	0.78 (0.30)	0.86 (0.15)	0.88 (0.11)	0.71 (0.34)	0.94 (0.10)	0.99 (0.04)
WUS	0.81 (0.62)	0.97 (0.18)	0.98 (0.13)	0.70 (0.81)	0.76 (0.51)	0.76 (0.46)	0.73 (0.74)	0.96 (0.21)	0.98 (0.14)
BC	Daily	Monthly	Yearly	Daily	Monthly	Yearly	Daily	Monthly	Yearly
US	0.80 (0.60)	0.95 (0.23)	0.98 (0.12)	0.68 (0.76)	0.80 (0.47)	0.84 (0.36)	0.78 (0.63)	0.95 (0.24)	0.98 (0.13)
EUS	0.81 (0.44)	0.94 (0.18)	0.98 (0.10)	0.65 (0.60)	0.73 (0.38)	0.77 (0.32)	0.78 (0.47)	0.94 (0.19)	0.97 (0.11)
CUS	0.80 (0.43)	0.94 (0.17)	0.98 (0.09)	0.70 (0.53)	0.82 (0.30)	0.86 (0.24)	0.77 (0.45)	0.94 (0.18)	0.97 (0.10)
WUS	0.77 (0.90)	0.95 (0.31)	0.98 (0.14)	0.67 (1.10)	0.80 (0.66)	0.86 (0.43)	0.75 (0.93)	0.95 (0.32)	0.98 (0.15)

Table S3. A summary of time periods, spatiotemporal resolutions, and overall accuracies of surface $PM_{2.5}$ and BC estimates focusing on the United States from previous studies.

Air pollutant	Model	Region	Time period	Temporal resolution	Spatial resolution	CV-R^2	Network	Literature
$PM_{2.5}$	Random Forest	US	2011	Daily	12 km	0.80	EPA AQS	[27]
	KC	US	2001-2006	Monthly	10 km	0.86	EPA AQS	[28]
	LUR + BME	US	2001-2006	Monthly	10 km	0.79	EPA AQS	[29]
	CNN	US	2011	Daily	10 km	0.84	EPA AQS	[30]
	GBT	US	2006-2020	Daily	10 km	0.65	EPA AQS	[31]
	Ensemble	WUS	2008-2018	Daily	Zip code	0.72	EPA, IMPROVE, Smoke	[17]
	GWR	US	2000-2016	Monthly	1 km	0.76	EPA + IMPROVE	[32]
	Neural Network	US	2000-2012	Daily	1 km	0.84	EPA AQS	[33]
	Ensemble	US	2000-2016	Daily	1 km	0.86	EPA AQS	[34]
	SWDF	**WUS**	**2000-2020**	**Daily**	**1 km**	**0.81**	EPA + IMPROVE	
		US		**Daily**	**1 km**	**0.82**	+ USFS	**This study**
		US		**Monthly**	**1 km**	**0.99**		
BC								
	Random Forest	US	2005-2015	Daily	> 25 km	0.75	IMPROVE + CSN	[35]
	GWR	US	2000-2016	Monthly	1 km	0.74	IMPROVE + CSN	[32]
	GEOS–Chem	US	2010	Annual	12 km	-	-	[36]
	SWDF		**2000-2020**	**Daily**	**1 km**	**0.80**	**IMPROVE + CSN**	**This study**
				Monthly	**1 km**	**0.94**		
				Annual	**1 km**	**0.96**		

CNN: convolutional neural network; GBT: gradient boosted trees; GWR: geographically weighted regression; KC: kriging $PM_{2.5}$ estimates based on the CSTM; LUR + NME: land use regression model and Bayesian maximum entropy model; STGK: space-time geostatistical kriging model; SWDF: spatiotemporally weighted deep forest

Appendix References

1. Wei J, Liu S, Li Z, et al. Ground-level NO_2 surveillance from space across China for high resolution using interpretable spatiotemporally weighted artificial intelligence. *Environ Sci Technol* 2022; **56**(14): 9988–98.
2. Anenberg SC, Horowitz LW, Tong DQ, West JJ. An estimate of the global burden of anthropogenic ozone and fine particulate matter on premature human mortality using atmospheric modeling. *Environ Health Perspect* 2010; **118**(9): 1189-95.
3. Ye T, Xu R, Yue X, et al. Short-term exposure to wildfire-related $PM_{2.5}$ increases mortality risks and burdens in Brazil. *Nat Commun* 2022; **13**(1): 7651.
4. Arranz MC, Moreno MFM, Medina AA, Capitán MA, Vaquer FC, Gómez AA. Health impact assessment of air pollution in Valladolid, Spain. *BMJ Open* 2014; **4**(10): e005999.
5. Murray CJL, Aravkin AY, Zheng P, et al. Global burden of 87 risk factors in 204 countries and territories, 1990-2019: a systematic analysis for the Global Burden of Disease Study 2019. *Lancet* 2020; **396**(10258): 1223-49.
6. Cohen AJ, Brauer M, Burnett R, et al. Estimates and 25-year trends of the global burden of disease attributable to ambient air pollution: an analysis of data from the Global Burden of Diseases Study 2015. *Lancet* 2017; **389**(10082): 1907-18.
7. Cai M, Lin X, Wang X, et al. Long-term exposure to ambient fine particulate matter chemical composition and in-hospital case fatality among patients with stroke in China. *Lancet Reg Health West Pac* 2023; **32**: 100679.
8. Bright EA, Coleman PR, Dobson JE. LandScan: a global population database for estimating populations at risk. *Photogramm Eng Rem S* 2000; **66**: 849-58.
9. Pope CA, Lefler JS, Ezzati M, et al. Mortality risk and fine particulate air pollution in a large, representative cohort of U.S. adults. *Environ Health Perspect* 2019; **127**(7): 077007.
10. Janssen NAH, Hoek G, Simic-Lawson M, et al. Black carbon as an additional indicator of the adverse health effects of airborne particles compared with PM_{10} and $PM_{2.5}$. *Environ Health Perspect* 2011; **119**(12): 1691-9.
11. Cermak J, Wild M, Knutti R, Mishchenko MI, Heidinger AK. Consistency of global satellite-derived aerosol and cloud data sets with recent brightening observations. *Geophys Res Lett* 2010; **37**(21): L21704.
12. Georgoulias AK, van der A RJ, Stammes P, Boersma KF, Eskes HJ. Trends and trend reversal detection in 2 decades of tropospheric NO_2 satellite observations. *Atmos Chem Phys* 2019; **19**(9): 6269-94.
13. Ichoku C, Ellison L. Global top-down smoke-aerosol emissions estimation using satellite fire radiative power measurements. *Atmos Chem Phys* 2014; **14**(13): 6643-67.
14. Wei J, Peng Y, Mahmood R, Sun L, Guo J. Intercomparison in spatial distributions and temporal trends derived from multi-source satellite aerosol products. *Atmos Chem Phys* 2019; **19**(10): 7183-207.
15. Watson JG, Chow JC, Moosmueller H, Green M, Frank N. Guidance for using continuous monitors in $PM_{2.5}$ monitoring networks. United States, 1998.
16. Solomon PA, Crumpler D, Flanagan JB, Jayanty RKM, Rickman EE, McDade CE. U.S. national $PM_{2.5}$ chemical speciation monitoring networks—CSN and IMPROVE: description of networks. *J Air Waste Manag Assoc* 2014; **64**(12): 1410-38.
17. Considine EM, Hao J, deSouza P, Braun D, Reid CE, Nethery RC. Evaluation of model-based $PM_{2.5}$ estimates for exposure assessment during wildfire smoke episodes in the Western U.S. *Environ Sci Technol* 2023; **57**(5): 2031-41.

18. Lyapustin A, Wang YJ, Korkin S, Huang D. MODIS Collection 6 MAIAC algorithm. *Atmos Meas Tech* 2018; **11**(10): 5741-65.
19. Garay MJ, Witek ML, Kahn RA, et al. Introducing the 4.4-km spatial resolution Multi-Angle Imaging SpectroRadiometer (MISR) aerosol product. *Atmos Meas Tech* 2020; **13**(2): 593-628.
20. Didan K. MODIS/Terra Vegetation Indices Monthly L3 Global 1km SIN Grid V061 [Data set]. *NASA EOSDIS Land Processes DAAC* 2021.
21. Farr TG, Rosen PA, Caro E, et al. The Shuttle Radar Topography Mission. *Rev Geophys* 2007; **45**(2): 2005RG000183.
22. Randles CA, da Silva AM, Buchard V, et al. The MERRA-2 aerosol reanalysis, 1980 onward. Part I: System description and data assimilation evaluation. *J Clim* 2017; **30**(17): 6823-50.
23. Buchard V, Randles CA, da Silva AM, et al. The MERRA-2 aerosol reanalysis, 1980 onward. Part II: Evaluation and case studies. *J Clim* 2017; **30**(17): 6851-72.
24. Crippa M, Guizzardi D, Muntean M, et al. Gridded emissions of air pollutants for the period 1970–2012 within EDGAR v4.3.2. *Earth Syst Sci Data* 2018; **10**(4): 1987-2013.
25. Muñoz-Sabater J, Dutra E, Agustí-Panareda A, et al. ERA5-Land: a state-of-the-art global reanalysis dataset for land applications. *Earth Syst Sci Data* 2021; **13**(9): 4349-83.
26. Hersbach H, Bell B, Berrisford P, et al. The ERA5 global reanalysis. *Q J R Meteorol Soc* 2020; **146**(730): 1999-2049.
27. Hu XF, Belle JH, Meng X, et al. Estimating $PM_{2.5}$ concentrations in the conterminous United States using the random forest approach. *Environ Sci Technol* 2017; **51**(12): 6936-44.
28. Lee SJ, Serre ML, van Donkelaar A, Martin RV, Burnett RT, Jerrett M. Comparison of geostatistical interpolation and remote sensing techniques for estimating long-term exposure to ambient $PM_{2.5}$ concentrations across the continental United States. *Environ Health Persp* 2012; **120**(12): 1727-32.
29. Beckerman BS, Jerrett M, Serre M, et al. A hybrid approach to estimating national scale spatiotemporal variability of $PM_{2.5}$ in the contiguous United States. *Environ Sci Technol* 2013; **47**(13): 7233-41.
30. Park Y, Kwon B, Heo J, Hu XF, Liu Y, Moon T. Estimating $PM_{2.5}$ concentration of the conterminous United States via interpretable convolutional neural networks. *Environ Pollut* 2020; **256**: 113395.
31. Childs ML, Li J, Wen J, et al. Daily local-level estimates of ambient wildfire smoke $PM_{2.5}$ for the contiguous US. *Environ Sci Technol* 2022; **56**(19): 13607-21.
32. van Donkelaar A, Martin RV, Li C, Burnett RT. Regional estimates of chemical composition of fine particulate matter using a combined geoscience-statistical method with information from satellites, models, and monitors. *Environ Sci Technol* 2019; **53**(5): 2595-611.
33. Di Q, Kloog I, Koutrakis P, Lyapustin A, Wang YJ, Schwartz J. Assessing $PM_{2.5}$ exposures with high spatiotemporal resolution across the continental United States. *Environ Sci Technol* 2016; **50**(9): 4712-21.
34. Di Q, Amini H, Shi LH, et al. An ensemble-based model of $PM_{2.5}$ concentration across the contiguous United States with high spatiotemporal resolution. *Environ Int* 2019; **130**: 104909.
35. Meng X, Hand JL, Schichtel BA, Liu Y. Space-time trends of $PM_{2.5}$ constituents in the conterminous United States estimated by a machine learning approach, 2005–2015. *Environ Int* 2018; **121**: 1137-47.
36. Li Y, Henze DK, Jack D, Henderson BH, Kinney PL. Assessing public health burden associated with exposure to ambient black carbon in the United States. *Sci Total Environ* 2016; **539**: 515-25.